Proc. Natl. Acad. Sci. USA
Vol. 96, pp. 1716–1721, February 1999
Neurobiology

Elimination of zinc from synaptic vesicles in the intact mouse brain by disruption of the *ZnT3* gene

TOBY B. COLE*, H. JÜRGEN WENZEL†, KATHY E. KAFER‡, PHILIP A. SCHWARTZKROIN†§, AND RICHARD D. PALMITER*‡¶

Departments of *Biochemistry, †Neurological Surgery, and §Physiology and Biophysics and ‡Howard Hughes Medical Institute, The University of Washington, Seattle, WA 98195

Contributed by Richard D. Palmiter, December 24, 1998

ABSTRACT **The mammalian protein ZnT3 resides on synaptic vesicle membranes of zinc-containing neurons, suggesting its possible role in vesicular zinc transport. We show here that histochemically reactive zinc, corresponding to the zinc found within synaptic vesicles, was undetectable in the brains of mice with targeted disruption of the *ZnT3* gene. Total zinc levels in the hippocampus and cortex of these mice were reduced by about 20%. The ultrastructure of mossy fiber boutons, which normally store the highest levels of vesicular zinc, was unaffected. Mice with one normal *ZnT3* allele had reduced levels of ZnT3 protein on synaptic vesicle membranes and had intermediate amounts of vesicular zinc. These results demonstrate that ZnT3 is required for transport of zinc into synaptic vesicles and suggest that vesicular zinc concentration is determined by the abundance of ZnT3.**

In the mammalian brain, 5–15% of total zinc is concentrated in synaptic vesicles in a subset of glutamatergic neurons (1–3), where it can be detected histochemically by using the neo-Timm sulfide silver method (4), with a selenium stain (5), or via the zinc-reactive fluorescent compound *N*-(6-methoxy-8-quinolyl)-*p*-toluene-sulfonamide (TSQ) (6). Histochemically reactive zinc is present in many regions of the central nervous system (7, 8) and is especially abundant in the hippocampus (7, 9, 10).

Despite the abundance of zinc in the brain (0.15–0.2 mM in gray matter) (8), little is known about the mechanisms controlling zinc homeostasis *in vivo*. Excess zinc may be sequestered by metallothioneins (11, 12), taken up into organelles (13), or transported out of the cell (14). Similarly, there are likely to be specific transport mechanisms regulating zinc influx. Under conditions of zinc toxicity, when extracellular zinc levels are high, zinc may enter into neurons via *N*-methyl-D-aspartate (NMDA) receptors, α-amino-3-hydroxy-5-methyl-4-isoxazolepropionic acid (AMPA)/kainate receptors, voltage-dependent calcium channels, or transporter-mediated exchange with intracellular sodium (15).

We recently identified a putative zinc transporter, ZnT3, that is expressed in zinc-containing neurons (16). ZnT3 belongs to a family of mammalian zinc transporters that includes ZnT1, a ubiquitously expressed zinc efflux er (14); ZnT2, which transports zinc into endosomal/lysosomal vesicles (13); and ZnT4, which is essential for regulating the zinc content of milk (17). ZnT3 is localized to the projections of zinc-containing neurons, producing an immunohistochemical staining pattern identical to that seen with the Timm stain for vesicular zinc (16, 18). ZnT3 immunoreactivity is evident on the membranes of zinc-rich (Timm-positive) synaptic vesicles (18). This localization, together with its homology to the vesicular zinc transporter, ZnT2 (16), suggested that ZnT3 might be responsible for the transport of zinc into synaptic vesicles. Here, we show that ZnT3 is required for zinc transport into synaptic vesicles and that vesicular zinc concentrations are sensitive to the amount of ZnT3 present on synaptic vesicle membranes.

MATERIALS AND METHODS

Generation of ZnT3 Knockout Mice. After isolating the *ZnT3* gene from a 129Sv mouse genomic library (16), a targeting vector was constructed by replacing a 4.3-kb *Stu*I-*Afl*II fragment encoding the first four exons with a cassette containing nuclear *lacZ* (*nlacZ*) and a neomycin-resistance gene (neo^r) driven by the *polII* promoter. Herpes simplex virus thymidine kinase (*TK*) genes were inserted 8 kb upstream at a *Not*I site and 1 kb downstream of the neo^r cassette at a *Nar*I site. Electroporation and selection of AB1 embryonic stem cells were performed as described previously (19), using 2 μM gancyclovir. Three correctly targeted colonies were identified by PCR, using primers in the *polII* promoter and exon 7 of *ZnT3*. Genotype was assessed routinely by duplicate DNA dot hybridization of tail DNA with probes that lie within the *ZnT3* deletion and in *nlacZ*. In some cases, Southern blot analysis of DNA digested with *Nhe*I was used to confirm genotypes, using a 380-bp *Taq*I/*Eco*RI probe complementary to the 3′ untranslated region of *ZnT3*. C57BL/129Sv hybrid mice of the F2 generation were used in all experiments.

Temporal and Spatial Expression of *ZnT3*. Western blotting was performed as described (16), using a 1:1,000 dilution of ZnT3 antiserum. *ZnT3* mRNA levels were determined by solution hybridization essentially as described (20), using a riboprobe complementary to the 3′ untranslated region of *ZnT3*. Unhybridized RNA was digested with RnaseA/RnaseT1 instead of S1 nuclease. Values are presented as molecules of mRNA per cell, assuming 6.4 pg DNA per diploid cell ($n = 4$ for each data point). Expression of *nlacZ* was determined by staining tissues with 5-bromo-4-chloro-3-indolyl-β D-galactoside (X-gal), as described (21). Before staining, the vertebral column was decalcified by incubating 3 days in decalcification solution (0.34 M sodium citrate/22.5% formic acid) at room temperature, with three changes of solution, then rinsed in running tap water overnight.

Elemental Analysis. Dissected brain regions were weighed, placed in acid-washed glass flasks, digested in 2 ml of ultrapure nitric acid (J. T. Baker), evaporated to dryness, and resuspended in 2.5 ml of 2% (vol/vol) nitric acid. Twelve elements (Al, As, B, Ca, Cu, Fe, K, Mg, Na, P, Si, and Zn) were assessed by inductively coupled plasma emission spectroscopy, using a Jarrel–Ash 955 spectrophotometer. Ag, Ba, Cd, Co, Cr, Mn, Ni, Pb, Se, and V were below detectable levels.

The publication costs of this article were defrayed in part by page charge payment. This article must therefore be hereby marked "*advertisement*" in accordance with 18 U.S.C. §1734 solely to indicate this fact.

PNAS is available online at www.pnas.org.

Abbreviations: ZnT3, zinc transporter 3; $ZnT3^{+/+}$, wild-type; $ZnT3^{+/-}$, heterozygous mutant; $ZnT3^{-/-}$, homozygous mutant; TSQ, N-(6-methoxy-8-quinolyl)-*p*-toluene-sulfonamide; s, stratum; MFB, mossy fiber bouton.

¶To whom reprint requests should be addressed. e-mail: palmiter@u.washington.edu.

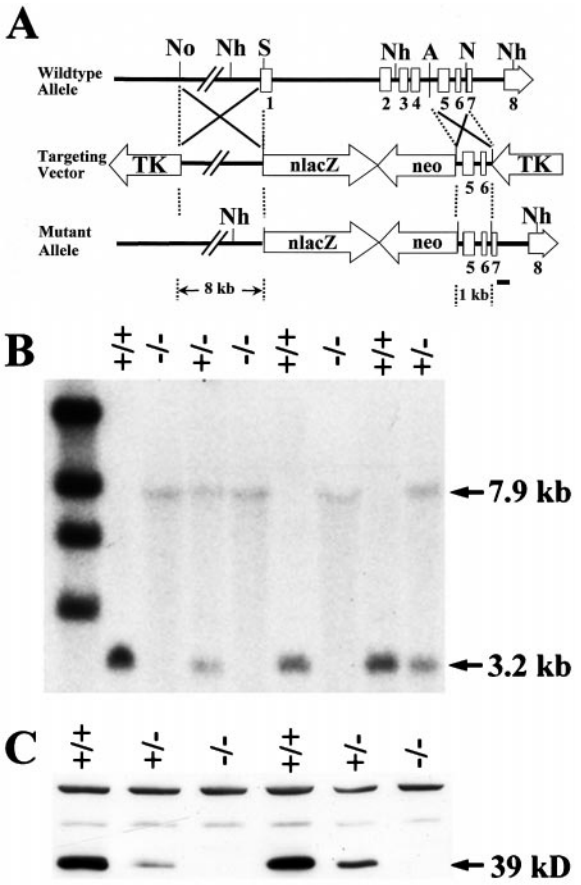

FIG. 1. Targeted disruption of the mouse *ZnT3* gene. (*A*) Diagram of the *ZnT3* wild-type allele, targeting vector, and predicted mutant allele. The targeting strategy placed *nlacZ* into the *ZnT3* locus, using *neo*^{r} for positive selection and herpes simplex virus thymidine kinase (*TK*) genes for negative selection. The eight numbered boxes represent exons. Homologous recombination in the regions indicated with an X should result in a mutant allele as shown at the bottom. The black bar represents the 380-bp *Taq*I/*Eco*RI probe used for Southern hybridization in *B*. A, *Afl*II; N, *Nar*I; Nh, *Nhe*I; No, *Not*I; S, *Stu*I. (*B*) Southern blot of *Nhe*I-digested genomic DNA from *ZnT3*$^{+/+}$, ZnT3$^{+/-}$, and ZnT3$^{-/-}$ mice. The probe detects a 7.9-kb mutant and 3.2-kb wild-type fragment. (*C*) Western blot of brain homogenates from 10-wk-old ZnT3$^{+/+}$, ZnT3$^{+/-}$, and ZnT3$^{-/-}$ mice. Equal amounts of total protein were loaded into each well. ZnT3 protein, which migrates as a 39-kD band, was undetectable in the brains of the mutants and reduced in the heterozygotes. The upper, nonspecific band controls for loading differences.

Tissue Processing for Timm Stain and Electron Microscopy. Brain tissue from 17 mice, ages 2–3 months, was processed for light microscopy and electron microscopy as described (18). The initial fixation was modified by using either 4% paraformaldehyde in 0.1 M sodium phosphate buffer, pH 7.4 (PB) (for immunocytochemistry), or 2% paraformaldehyde/2% glutaraldehyde in 0.1 M PB (for electron microscopy).

Immunocytochemistry. ZnT3 and dynorphin immunocytochemistry were performed as described (18, 22). To quantify ZnT3 immunoreactivity, film negatives of stained sections were analyzed by using IMAGETOOL (University of Texas Health Science Center, San Antonio, available at hyperlink ftp://maxrad6.uthscsa.edu) to measure average gray-scale values of selected regions. Data are presented as mean ± SEM of 16 sections for each genotype. For glutamate immunocytochemistry, a rabbit antiglutamate antibody (Sigma) was used (1:10,000 dilution), followed by goat-anti-rabbit IgG conjugated to gold (10 nm, Ted Pella, Redding, CA) (1:20 dilution).

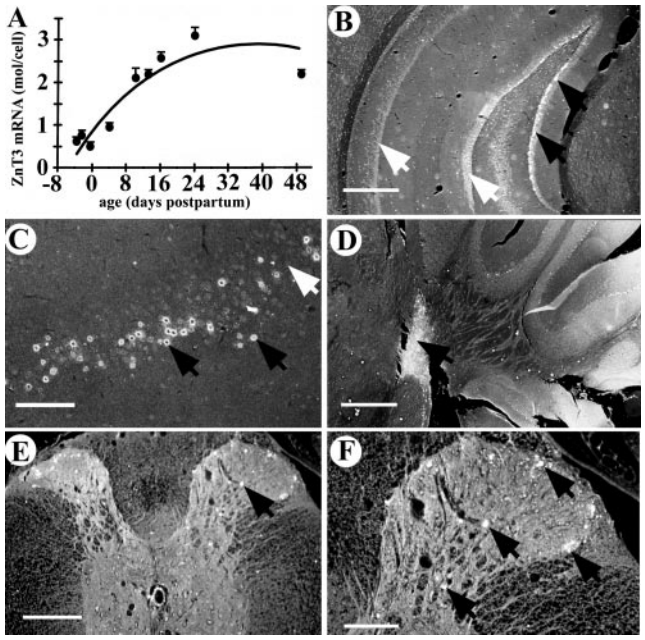

FIG. 2. ZnT3 is expressed in the central nervous system. (*A*) ZnT3 mRNA levels in developing mouse brain, assessed by solution hybridization. Data are presented as mean ± SEM. (B–F) Expression of *nlacZ* (under the control of the ZnT3 promoter) in the central nervous system of *ZnT3*$^{+/-}$ mice, as detected by 5-bromo-4-chloro-3-indolyl-β D-galactoside (X-gal) staining (white nuclei, indicated by black arrows). nlacZ is expressed in s granulosum of the dentate gyrus (*B*), the pyriform cortex (*C*), and the cochlear nucleus (*D*). *nlacZ* expression was not completely penetrant, as evident by the absence of staining (white arrows) in many areas where *ZnT3* is normally expressed. (*E* and *F*) *nlacZ* is expressed in laminae I, II, III, and IV of the spinal cord dorsal horn. Sections were photographed under dark-field illumination. [Bars = 500 μm (*B* and *D*); 200 μm (*C* and *E*); 100 μm (*F*).]

Timm Stain. Timm staining was performed by immersion in sulfide solution (18). The method described was modified slightly. After the initial perfusion with 4% paraformaldehyde in 0.1 M PB, brains were immersed in 3% glutaraldehyde/0.1% Na_2S/0.136 mM $CaCl_2$ in 0.12 M Millonig's buffer, pH 7.3 for 48 hr at 4°C. The tissue was transferred to cold 0.12 M Millonig's buffer with 0.136 mM $CaCl_2$, then cryoprotected, frozen on dry ice, cut into 30-μm sections, and mounted on gelatin-coated slides. Sections were immersed in developer [30 ml gum Arabic (50%)/5 ml citrate buffer (2 M, pH 3.7)/15 ml hydroquinone (5.67%)/0.25 ml $AgNO_3$ (17%)] for 60–90 min.

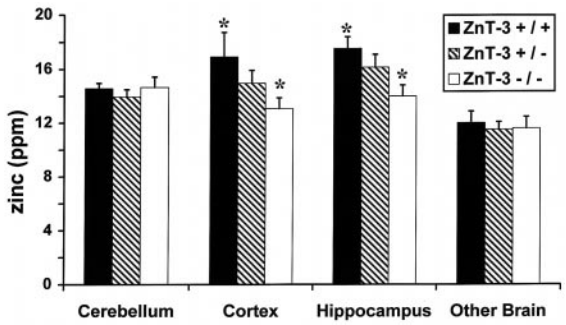

FIG. 3. Total zinc is reduced in the hippocampus and cortex of *ZnT3*$^{-/-}$ mice. Selected regions of the brain were dissected, and elemental analysis was performed for 22 elements, including zinc (see Materials and Methods). Total zinc was reduced by about 20% in the hippocampus and cortex of *ZnT3*$^{-/-}$ mice, and ZnT3$^{+/-}$ mice had a 10% reduction in total zinc in these same regions. Data are presented as mean ± SEM (n = 4).

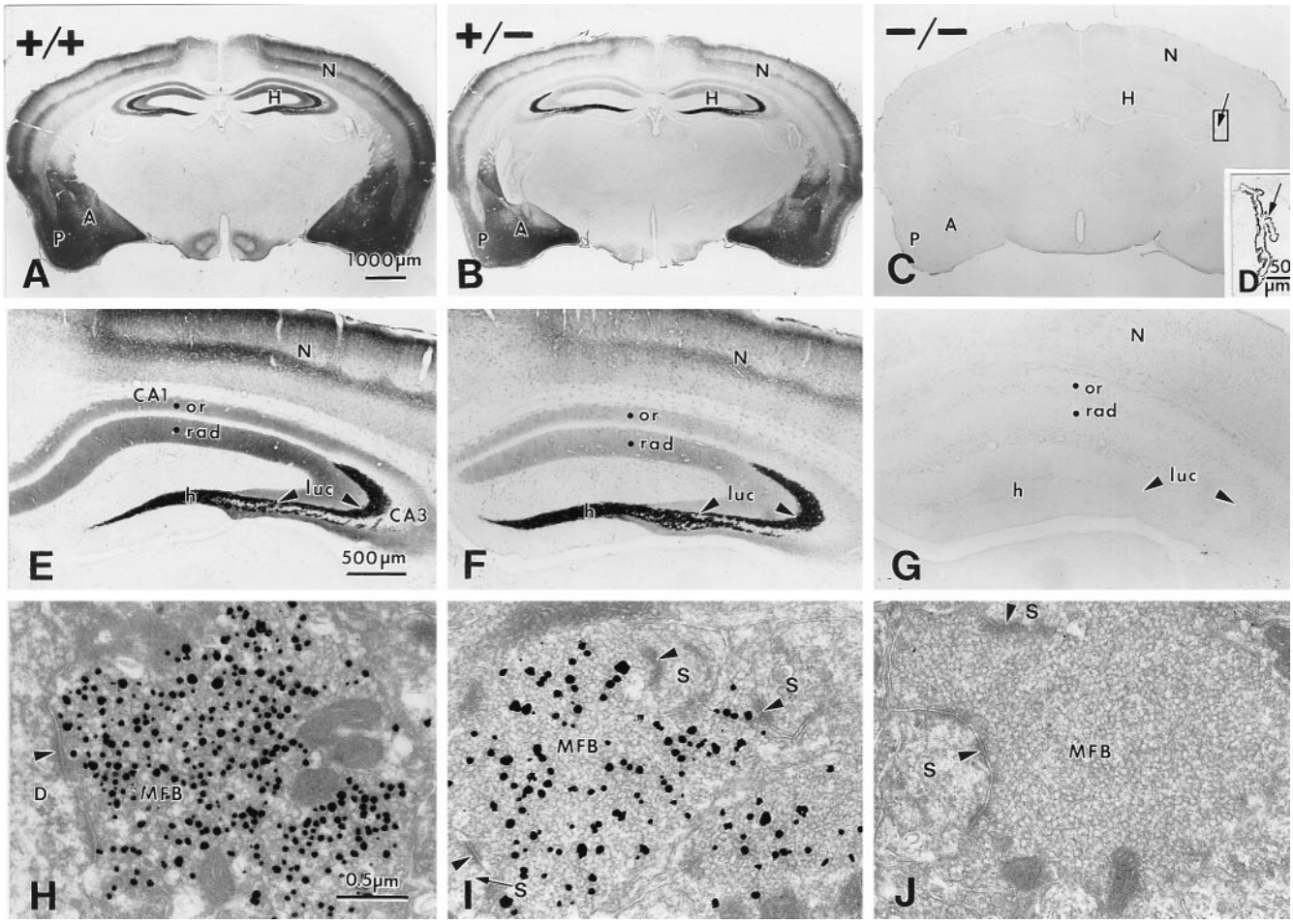

FIG. 4. Timm stain is undetectable in the brains of $ZnT3^{-/-}$ mice. Comparison of Timm stain between brains of $ZnT3^{+/+}$ (*A, E,* and *H*), *ZnT-3*$^{+/-}$ (*B, F,* and *I*), and *ZnT-3*$^{-/-}$ mice (*C, G,* and *J*). (*A–C*) Coronal sections through the midbrain. Timm stain in the hippocampus (*H*), piriform cortex (P), neocortex (N), and amygdala (A) was conspicuous in the $ZnT3^{+/+}$ brain (*A*), reduced in the $ZnT3^{+/-}$ brain (*B*), and undetectable in the brains of $ZnT3^{-/-}$ mice (*C*). (*D*) Higher magnification of the choroid plexus from the lateral ventricle (indicated area in *C*). Timm stain was unperturbed in the $ZnT3^{-/-}$ choroid plexus. (*E–G*) Higher magnification of Timm-stained hippocampi from $ZnT3^{+/+}$ (*E*), $ZnT3^{+/-}$ (*F*), and $ZnT3^{-/-}$ (*G*) mice. Timm stain was reduced ($ZnT3^{+/-}$) or absent ($ZnT3^{-/-}$) in the hilus (h), s lucidum (luc) of CA3, and s oriens (or) and s radiatum (rad) of CA1 and CA3. (*H–J*) Electron micrographs of Timm-stained MFBs in s lucidum of CA3, taken from a $ZnT3^{+/+}$ (*H*), a $ZnT3^{+/-}$ (*I*), and a $ZnT3^{-/-}$ (*J*) mouse. Timm-positive vesicles were abundant in $ZnT3^{+/+}$ MFBs, whereas fewer vesicles were Timm-positive in $ZnT3^{+/-}$ MFBs, and no Timm-positive vesicles were present in $ZnT3^{-/-}$ MFBs. Arrowheads represent synaptic contacts made with a dendrite (D) and dendritic spines (S).

For ultrastructural analysis, Timm staining was performed as described (18).

***N*-(6-Methoxy-8-quinolyl)-*p*-Toluene-Sulfonamide (TSQ) Histofluorescence.** A working solution of TSQ (Molecular Probes), prepared as described (6, 23), was pipetted onto unfixed frozen brain sections. Hippocampi were scanned under UV illumination (351–362 nm) with an ACAS 570 laser cytometer (Meridian Instruments, Lansing, MI). Emissions >370 nm were recorded, and images were analyzed on a DASY 9000 workstation (Meridian). Average fluorescence for selected regions was measured, then converted to percentage of maximal fluorescence, which was observed in the wild-type hilus. Regions selected for analysis included the hilus, CA3 [stratum (s) oriens and s lucidum], CA1 (s radiatum, s oriens, and s pyramidale), and a small section of the dorsomedial thalamus just beneath the dentate area of the hippocampus. Fluorescence was quantified from two coronal sections each of the left and right hippocampi of five mice. Frozen sections of mouse testis and pancreas were air-dried, fixed in ice-cold methanol, and stained with TSQ as above. Fluorescence was visualized and photographed with a Nikon Microphot FX microscope, using a UV-2A filter block (excitation, 330–380 nm; barrier, 420 nm).

RESULTS

Disruption of the Murine *ZnT3* Gene. The first four exons of *ZnT3* were replaced by a cassette that included *nlacZ* and *neo*^{r} (Fig. 1*A*). This construct was electroporated into embryonic stem cells. PCR analysis of 60 clones revealed three that were targeted correctly. One of these produced chimeras that transmitted the targeted allele through the germ line. F1 heterozygotes were generated by crossing the chimeras with C57BL/6 females. The F2 progeny from these mice, genotyped by duplicate DNA dot hybridization or by Southern blot analysis (Fig. 1*B*), were born in the expected Mendelian ratio. Mice heterozygous ($ZnT3^{+/-}$) or homozygous ($ZnT3^{-/-}$) for the disrupted allele showed no obvious phenotypic differences from their wild-type ($ZnT3^{+/+}$) littermates. Body weight, lifespan, fertility, and litter size were normal, and the mice showed no gross morphological abnormalities. ZnT3 protein, assessed by Western blot analysis of brain homogenates, was reduced in the brains of $ZnT3^{+/-}$ mice and undetectable in the brains of $ZnT3^{-/-}$ mice (Fig. 1*C*).

Insertion of *nlacZ* into the *ZnT3* locus confirmed the patterns of *ZnT3* expression seen previously by *in situ* hybridization (16), including expression in granule cells of the dentate gyrus, pyramidal cells of the CA3 and CA1 regions,

and the amygdala, neocortex, and piriform and entorhinal cortices (Fig. 2 *B* and *C*; data not shown for all regions). In addition, *nlacZ* expression was detected in the cochlear nucleus (Fig. 2*D*), laminae I–IV of the dorsal horn of the spinal cord (Fig. 2 *E* and *F*), and the testis, where ZnT3 mRNA is abundant but not translated into protein (16). ZnT3 mRNA, isolated from the brains of wild-type embryos or pups and quantified by solution hybridization, was negligible at birth, then increased linearly, reaching a maximum at about 3 weeks postpartum (Fig. 2*A*).

Vesicular Zinc Is Eliminated from Brains of *ZnT3*$^{-/-}$ Mice. To determine whether the levels of zinc or other metals were altered upon disruption of *ZnT3*, metal content was measured by plasma emission spectroscopy (Fig. 3). In the hippocampus and cortex, regions that contain abundant vesicular zinc (8), total zinc was reduced in the *ZnT3*$^{-/-}$ mice by 20% ($P < 0.001$, Student's *t* test) and 23% ($P < 0.01$), respectively, whereas the cerebellum and other (primarily thalamus and hypothalamus) regions without appreciable levels of vesicular zinc were unaffected (Fig. 3). Total zinc levels in the hippocampus and cortex of the *ZnT3*$^{+/-}$ mice were reduced by 10% ($P < 0.05$, Student's *t* test) (Fig. 3). None of the other 11 elements tested (see *Materials and Methods*) showed any change in abundance.

To test whether vesicular zinc is altered in these mice, we used two stains for histochemically reactive zinc, Timm stain and TSQ fluorescence. Timm stain was reduced in the brains of *ZnT3*$^{+/-}$ mice and eliminated from the brains of *ZnT3*$^{-/-}$ mice, including the staining normally seen in the hippocampus, neocortex, piriform cortex, amygdala (Fig. 4 *A–C*), entorhinal cortex, striatum, olfactory bulb, and cochlear nucleus (data not shown). In the hippocampus, Timm stain was reduced (*ZnT3*$^{+/-}$) or undetectable (*ZnT3*$^{-/-}$) in the mossy fibers projecting from dentate granule neurons to the hilus and s lucidum and s oriens of the CA3 region, and in projections to s radiatum and s oriens of the CA1 region (Fig. 4 *E–G*). Timm stain was undetectable in the *ZnT3*$^{-/-}$ brain even after long histochemical-development times (>90 min) that normally produce intense staining in CA1 and prominent staining in the inner and outer molecular layers of the dentate gyrus (data not shown). In contrast, Timm stain was readily detectable in the choroid plexus (Fig. 4*D*) and in convoluted tubule cells of the submaxillary gland (data not shown). At the ultrastructural level, Timm reaction product was present within synaptic vesicles of mossy fiber boutons (MFBs) in the *ZnT3*$^{+/+}$ brain (Fig. 4*H*), whereas the number of Timm-positive vesicles in *ZnT3*$^{+/-}$ MFBs was reduced (Fig. 4*I*), and no Timm-staining was detected within synaptic vesicles of *ZnT3*$^{-/-}$ MFBs (Fig. 4*J*), indicating that histochemically reactive zinc is eliminated from synaptic vesicles in the brains of *ZnT3*$^{-/-}$ mice.

Vesicular Zinc Content Is Determined by the Abundance of ZnT3 on Synaptic Vesicle Membranes. To investigate whether the amount of ZnT3 present on vesicle membranes was reduced in the *ZnT3*$^{+/-}$ brain, we assessed ZnT3 immunoreactivity in the brains of *ZnT3*$^{+/+}$, *ZnT3*$^{+/-}$, and *ZnT3*$^{-/-}$ mice at the light-microscopic and ultrastructural levels (Fig. 5). ZnT3 immunoreactivity in the *ZnT3*$^{+/+}$ brain was evident in the same areas reported previously (16, 18). In the corresponding regions of the mutant brain, ZnT3 immunoreactivity was reduced (*ZnT3*$^{+/-}$) or undetectable (*ZnT3*$^{-/-}$), including the amygdala, cortex, and hippocampus (for hippocampus, see Fig. 5 *A, C,* and *E*; other regions, data not shown). ZnT3 immunoreactivity in the hippocampi of *ZnT3*$^{+/+}$, *ZnT3*$^{+/-}$, and *ZnT3*$^{-/-}$ mice was quantified by computer-assisted gray-scale analysis of film negatives (low gray-scale values correspond to darker ZnT3 immunostaining). In the *ZnT3*$^{+/-}$ hippocampus, gray-scale values relative to the corpus callosum were intermediate in the hilus (*ZnT3*$^{+/+}$, 0.35 ± 0.03; *ZnT3*$^{+/-}$, 0.50 ± 0.02; *ZnT3*$^{-/-}$, 0.83 ± 0.05) and s lucidum of CA3 (*ZnT3*$^{+/+}$, 0.39 ± 0.04; *ZnT3*$^{+/-}$, 0.54 ± 0.02; *ZnT3*$^{-/-}$, 0.81 ± 0.05). At the ultrastructural level, ZnT3 immunoreactivity was present on all synaptic vesicles within *ZnT3*$^{+/-}$ MFBs, similarly as in the *ZnT3*$^{+/+}$ MFBs, but the intensity of ZnT3 immunoreactivity was reduced (compare Fig. 5 *B* and *D*). ZnT3 immunoreactivity was undetectable in MFBs of *ZnT3*$^{-/-}$ mice (Fig. 5*F*).

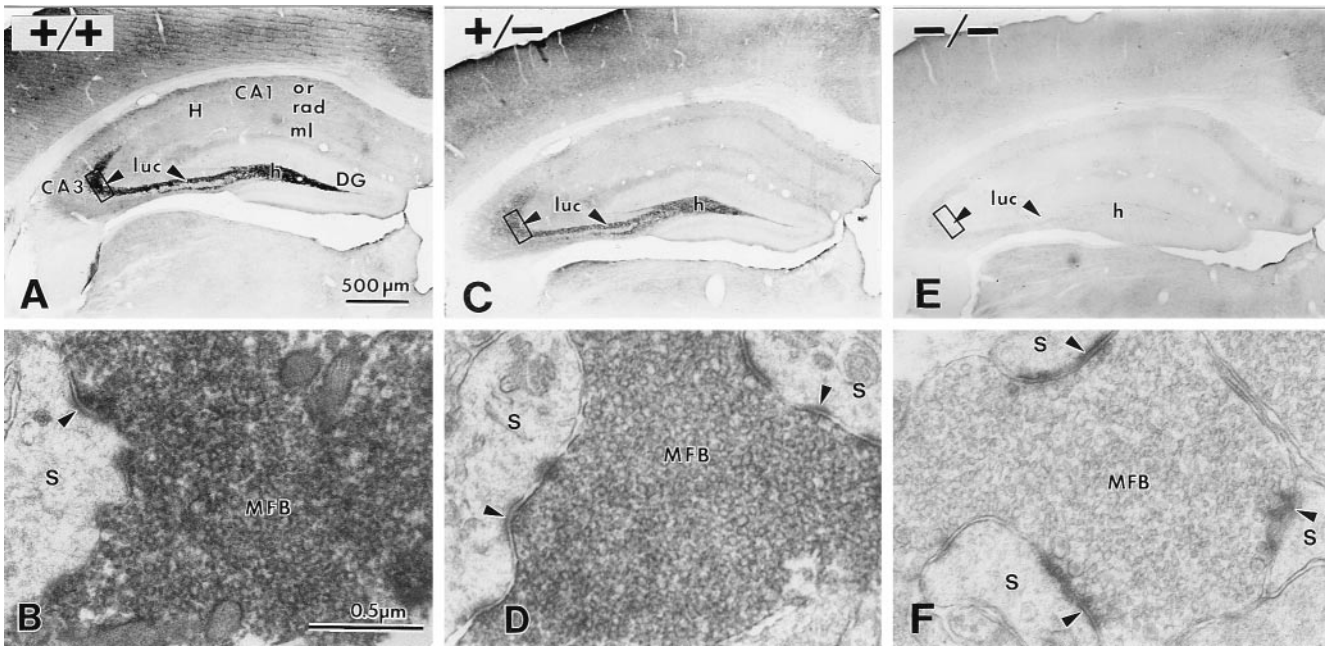

FIG. 5. ZnT3 immunocytochemistry in the *ZnT3*$^{+/+}$ (*A* and *B*), *ZnT3*$^{+/-}$ (*C* and *D*), and *ZnT3*$^{-/-}$ (*E* and *F*) hippocampus. Compared with the *ZnT3*$^{+/+}$ hippocampus (*A*), ZnT3 immunoreactivity was reduced in many areas of the *ZnT3*$^{+/-}$ hippocampus (*C*) and was undetectable in the *ZnT3*$^{-/-}$ hippocampus (*E*). (*B, D,* and *F*) Electron micrographs of MFBs in s lucidum (boxed area in *A, C,* and *E*). ZnT3 immunoreactivity was conspicuous on synaptic vesicle membranes of *ZnT3*$^{+/+}$ MFBs (*B*), reduced on vesicle membranes of ZnT3$^{+/-}$ MFBs (*D*), and undetectable on vesicle membranes of ZnT3$^{-/-}$ MFBs (*F*). The number of immunoreactive vesicles in the ZnT3$^{+/-}$ and ZnT3$^{+/+}$ MFBs was approximately the same. Arrowheads point to synaptic contacts made with dendritic spines (S). H, hippocampus; DG, dentate gyrus; h, hilus; luc, s lucidum; or, s oriens; rad, s radiatum; ml, molecular layer.

TSQ fluorescence, a specific indicator of vesicular zinc, was used to corroborate the results seen with Timm stain and to provide a quantitative comparison of vesicular zinc levels in the hippocampi of *ZnT-3*$^{+/+}$, *ZnT-3*$^{+/-}$, and *ZnT-3*$^{-/-}$ mice. TSQ fluorescence was undetectable in the *ZnT3*$^{-/-}$ hippocampus (Fig. 6*A*), but still abundant in differentiating spermatids in the testis and in β-islet cells of the pancreas (Fig. 6 *C* and *D*). TSQ fluorescence was quantified, using computer-assisted laser cytometry, from several regions of the hippocampus and a small region within the dorsomedial thalamus (Fig. 6*B*). Average fluorescence for each region was plotted as a percentage of the maximal fluorescence, which was seen in the wild-type hilus. TSQ fluorescence in the hilus and regions CA3 and CA1 was absent in the *ZnT3*$^{-/-}$ hippocampus ($P < 0.0001$, Student's *t* test), where it was even lower than the background fluorescence, i.e., that seen in the thalamus or corpus callosum (Fig. 6 *A* and *B*). TSQ fluorescence in the *ZnT3*$^{+/-}$ hippocampus was reduced by 47% in the hilus, 39% in region CA3, and 50% in region CA1 ($P < 0.0001$ for all regions, Student's *t* test) (Fig. 6*B*).

Ultrastructural Morphology of the *ZnT3*$^{-/-}$ Hippocampus Is Normal. Examination of the hippocampi of adult *ZnT3*$^{-/-}$ mice by light microscopy revealed no grossly aberrant morphology. Stratum granulosum of the dentate gyrus and strata pyramidale, oriens, and radiatum of the CA3 and CA1 regions were normal in appearance, and mossy fiber projections were evident in s lucidum and s oriens of CA3, as detected by dynorphin immunoreactivity (data not shown). Ultrastructural analysis revealed the *ZnT3*$^{-/-}$ hippocampus to be normal with respect to the relative number, distribution, and size of MFBs in the hilus and s lucidum, as well as the number of synaptic vesicles contained within the MFBs, the number of asymmetric synaptic contacts made with dendritic spines (Fig. 7), and the presence of glutamate immunoreactivity (data not shown). MFBs in the *ZnT3*$^{-/-}$ hippocampus showed normal characteristic ultrastructure, with densely packed clear, round synaptic vesicles, a few dense core vesicles, and numerous mitochondria (Fig. 7), lacking only histochemically reactive zinc within the synaptic vesicles (Fig. 4*J*).

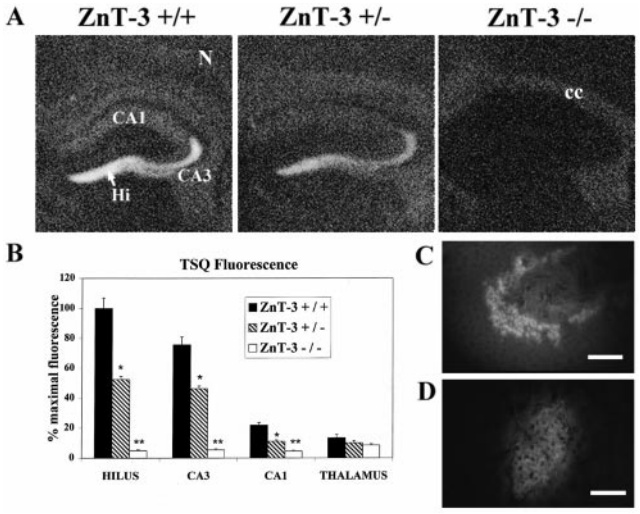

FIG. 6. TSQ fluorescence in the hippocampus. (*A*) Computer-generated images of TSQ fluorescence in the hippocampi of *ZnT3*$^{+/+}$ (*Left*), *ZnT3*$^{+/-}$ (*Center*), and *ZnT3*$^{-/-}$ (*Right*) mice. The bright fluorescence in the hilus (Hi), s oriens and s lucidum of CA3, and s oriens and s radiatum of CA1 was reduced in the *ZnT3*$^{+/-}$ hippocampus and undetectable in the *ZnT3*$^{-/-}$ hippocampus. TSQ staining was also reduced in the neocortex (N). TSQ fluorescence in the hippocampus of the mutants was less than the autofluorescence of the overlying corpus callosum (cc). (*B*) Quantification of TSQ fluorescence in regions within the hippocampus by computer-assisted laser cytometry. Data are expressed as mean ± SEM ($n = 5$). (*C*) TSQ-stained section of a single seminiferous tubule from the testis of a *ZnT3*$^{-/-}$ mouse. Spermatids poised at the lumen of the tubule fluoresced with TSQ, similar to wild-type spermatids (not shown). (*D*) TSQ-stained pancreas from a *ZnT3*$^{-/-}$ mouse, illustrating a single Islet of Langerhans, composed of beta cells that have an abundance of histochemically reactive zinc packaged in secretory granules. [Bars = 50 μm (*C*); 100 μm (*D*).]

DISCUSSION

Together with our previous observations (18), these studies indicate that zinc is taken up into synaptic vesicles by a transport mechanism that requires ZnT3 at the vesicle membrane. Histochemically reactive zinc was undetectable in the brains of *ZnT3*$^{-/-}$ mice, and there was a corresponding 20% reduction in total zinc in brain regions in which histochemically reactive zinc is usually detected. The remaining 80% of zinc in these regions represents zinc that is inaccessible to either sulfide or TSQ, presumably because of its tight association with metalloproteins in different parts of the cell. The results are consistent with previous studies suggesting that Timm stain and TSQ fluorescence throughout the brain correspond exclusively to zinc that is packaged into synaptic vesicles (8).

The *ZnT3*$^{+/-}$ brain had an intermediate level of both ZnT3 protein and histochemically reactive zinc, demonstrating that the amount of zinc in synaptic vesicles is limited by the abundance of ZnT3. This variation in ZnT3 immunoreactivity extended to the ultrastructural level, where the intensity of ZnT3 immunoreactivity on synaptic vesicle membranes in *ZnT3*$^{+/-}$ MFBs was reduced relative to that seen in *ZnT3*$^{+/+}$ MFBs, but the number of ZnT3 immunoreactive vesicles remained unchanged. The sensitivity of vesicular zinc levels to the amount of ZnT3 present on synaptic vesicle membranes is consistent with a steady-state model for the regulation of zinc content in synaptic vesicles. In such a model, vesicular zinc content is determined by steady-state balance between influx and efflux, rather than a predetermined "set point." Only steady-state mechanisms are predicted to be sensitive to the amount of transporter (ZnT3) present on the vesicle membrane (24). ZnT3 is similar to other synaptic vesicle transporters in this regard (25, 26).

ZnT3 transports zinc into vesicles against a high concentration gradient, but the driving force is not clear. ZnT3 may act as part of a complex of proteins that mediate zinc transport. ZnT3 appears to depend on the AP-3 vesicular chaperone complex for assembly into synaptic vesicles because *mocha* mice, which lack the δ-subunit of this complex, have reduced ZnT3 immunoreactivity in the hippocampus (27). Interestingly, the phenotype of *mocha* mice, which includes hypopigmentation, defects in hearing and neural activity, and platelet storage pool deficiencies, in addition to reduced vesicular zinc,

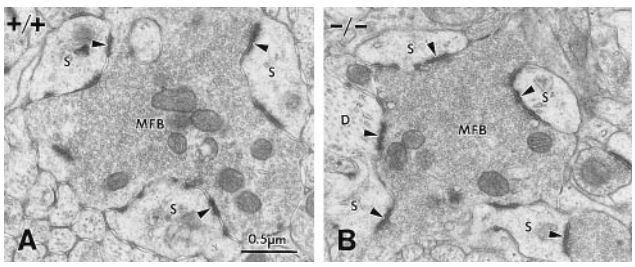

FIG. 7. MFBs in the ZnT3$^{-/-}$ hippocampus show normal ultrastructure. Electron micrographs of MFBs in s lucidum of CA3, taken from a ZnT3$^{+/+}$ (*A*) and a ZnT3$^{-/-}$ (*B*) mouse. ZnT3$^{-/-}$ MFBs were normal with respect to their size, the approximate number of small, clear synaptic vesicles contained within them, the numbers and types of synaptic contacts made with dendritic spines, and the presence of mitochondria. Note the asymmetric synaptic contacts (arrowheads) on dendritic spines (S) and a pyramidal cell dendrite (D).

is much more severe than that seen in $ZnT3^{-/-}$ mice, as would be expected if AP-3 is involved in the assembly of many vesicular components. The hypersynchronized theta rhythms, spontaneous bursts of epileptiform activity, and loss of hearing seen in *mocha* mice (27, 28) are not likely to be due exclusively to the loss of vesicular zinc, because $ZnT3^{-/-}$ mice can still hear more than a year after birth, and they manifest normal electroencephalographic activity (our unpublished observations).

ZnT3 is required for sequestration of zinc in synaptic vesicles of neurons, whereas removal of ZnT3 did not affect the histochemically reactive zinc found in secretory granules of pancreatic β-islet cells (29), salivary gland granular convoluted tubule cells (30), germ cells in the testis (31, 32), or cuboidal cells of the choroid plexus (8). Other members of the ZnT family are likely to be responsible for compartmentalization of zinc in these and other cells.

Zinc is found solely in synaptic vesicles of glutamatergic neurons, but not all glutamatergic neurons sequester zinc (8). This observation, as well as the results presented here, suggest that zinc is not required for utilization of glutamate as a neurotransmitter. Given the many potential neuromodulatory and neurotoxic roles of synaptically released zinc (33–35), it will be interesting to see whether neuronal activity or excitotoxic damage is altered in these mice. If zinc does act as a neuromodulator, we predict that there will be a mechanism for clearing zinc from the synapse (probably a reuptake transporter) and a mechanism for shuttling zinc back into synaptic vesicles. Members of the ZIP (36) family of metal ion uptake transporters and the zinc-binding protein metallothionein-III, which is expressed in zinc-containing neurons (11), are possible candidates for some of these processes.

We thank Norma Anderson for assistance with electron microscopy, Glenda Froelick for assistance with histology, Terrance Kavanaugh for assistance with laser cytometry, Jeff Noebels and Margit Burmeister for communication of results before publication, and members of the Palmiter and Schwartzkroin labs for valuable discussions. This work was supported in part by National Institutes of Health Grants DK53013 (R.D.P.) and NS18895 (P.A.S.) and a U.S. Public Health Service National Research Service Award (T32 GM07270 to T.B.C.).

1. Haug, F. M. (1967) *Histochemie* **8,** 355–368.
2. Pérez-Clausell, J. & Danscher, G. (1985) *Brain Res.* **337,** 91–98.
3. Frederickson, C. J. & Moncrieff, D. W. (1994) *Biol. Signals* **3,** 127–139.
4. Danscher, G. (1981) *Histochemistry* **71,** 1–16.
5. Danscher, G. (1984) in *The Neurobiology of Zinc*, eds. Frederickson, C. J., Kasarskis, E. J. & Howell, G. A. (Liss, New York), Vol. B, pp. 177–191.
6. Frederickson, C. J., Kasarskis, E. J., Ringo, D. & Frederickson, R. E. (1987) *J. Neurosci. Methods* **20,** 91–103.
7. Slomianka, L. (1992) *Neuroscience* **48,** 325–352.
8. Frederickson, C. J. (1989) *Int. Rev. Neurobiol.* **31,** 145–238.
9. Crawford, I. L. & Connor, J. D. (1972) *J. Neurochem.* **19,** 1451–1458.
10. Zimmer, J. & Haug, F. M. (1978) *J. Comp. Neurol.* **179,** 581–617.
11. Erickson, J. C., Hollopeter, G., Thomas, S. A., Froelick, G. J. & Palmiter, R. D. (1997) *J. Neurosci.* **17,** 1271–1281.
12. Maret, W. (1995) *Neurochem. Int.* **27,** 111–117.
13. Palmiter, R. D., Cole, T. B. & Findley, S. D. (1996) *EMBO J.* **15,** 1784–1791.
14. Palmiter, R. D. & Findley, S. (1995) *EMBO J.* **14,** 639–649.
15. Sensi, S. L., Canzoniero, L. M. T., Yu, S. P., Ying, H., Koh, J. Y., Kerchner, G. A. & Choi, D. W. (1997) *J. Neurosci.* **17,** 9554–9564.
16. Palmiter, R. D., Cole, T. B., Quaife, C. J. & Findley, S. D. (1996) *Proc. Natl. Acad. Sci. USA* **93,** 14934–14939.
17. Huang, L. & Gitschier, J. (1997) *Nat. Genet.* **17,** 292–297.
18. Wenzel, H. J., Cole, T. B., Born, D. E., Schwartzkroin, P. A. & Palmiter, R. D. (1997) *Proc. Natl. Acad. Sci. USA* **94,** 12676–12681.
19. Thomas, S. A., Matsumoto, A. M. & Palmiter, R. D. (1995) *Nature (London)* **374,** 643–646.
20. Durnam, D. M. & Palmiter, R. D. (1983) *Anal. Biochem.* **131,** 385–393.
21. Masters, B. A., Quaife, C. J., Erickson, J. C., Kelly, E. J., Froelick, G. J., Zambrowicz, B. P., Brinster, R. L. & Palmiter, R. D. (1994) *J. Neurosci.* **14,** 5844–5857.
22. Houser, C. R., Miyashiro, J. E., Swartz, B. E., Walsh, G. O., Rich, J. R. & Delgado-Escueta, A. V. (1990) *J. Neurosci.* **10,** 267–282.
23. Erickson, J. C., Masters, B. A., Kelly, E. J., Brinster, R. L. & Palmiter, R. D. (1995) *Neurochem. Int.* **27,** 35–41.
24. Williams, J. (1997) *Neuron* **18,** 683–686.
25. Takahashi, N., Miner, L. L., Sora, I., Ujike, H., Revay, R. S., Kostic, V., Jackson-Lewis, V., Przedborski, S. & Uhl, G. R. (1997) *Proc. Natl. Acad. Sci. USA* **94,** 9938–9943.
26. Song, H., Ming, G., Fon, E., Bellochio, E., Edwards, R. H. & Poo, M. (1997) *Neuron* **18,** 815–826.
27. Kantheti, P., Qiao, X., Diaz, M. E., Peden, A. A., Meyer, G. E., Carskadon, S. L., Kapfhamer, D., Sufalko, D., Robinson, M. S., Noebels, J. L. & Burmeister, M. (1998) *Neuron* **21,** 111–122.
28. Noebels, J. L. & Sidman, R. L. (1989) *J. Neurogenet.* **6,** 53–56.
29. Toroptsev, I. V., Eschenko, V. A. & Troshkin, V. G. (1974) *Bull. Exp. Biol. Med.* **77,** 119–121.
30. Frederickson, C. J., Pérez-Clausell, J. & Danscher, G. (1987) *J. Histochem. Cytochem.* **35,** 579–583.
31. Danscher, G. & Zimmer, J. (1978) *Histochemistry* **55,** 27–40.
32. Andrews, J. C., Nolan, J. P., Hammerstedt, R. H. & Bavister, B. D. (1995) *Cytometry* **21,** 153–159.
33. Choi, D. W. & Koh, J. Y. (1998) *Annu. Rev. Neurosci.* **21,** 347–375.
34. Harrison, N. L. & Gibbons, S. J. (1994) *Neuropharmacology* **33,** 935–952.
35. Smart, T. G., Xie, X. & Krishek, B. J. (1994) *Prog. Neurobiol.* **42,** 393–441.
36. Eng, B. H., Guerinot, M. L., Eide, D. & Saier, M. H., Jr. (1998) *J. Membrane Biol.* **166,** 1–7.